

## SCATTER STRATEGIES FOR CLUSTER FLIGHT

**Dr. Brenton Duffy**<sup>(1)</sup>, **Allen G. Brown**<sup>(2)</sup>, **Dr. Matthew C. Ruschmann**<sup>(3)</sup>, and **Lucas Ward**<sup>(4)</sup>  
(1,2,3,4)*Emergent Space Technologies Inc., 6411 Ivy Lane, Greenbelt, MD 20770, (301) 345-1535*

<sup>(1)</sup>*brenton.duffy@emergentspace.com*

<sup>(2)</sup>*allen.brown@emergentspace.com*

<sup>(3)</sup>*matthew.ruschmann@emergentspace.com*

<sup>(4)</sup>*lucas.ward@emergentspace.com*

**Abstract:** *Emergent Space Technologies has developed robust and scalable cluster flight guidance, navigation, and control flight simulation software that optimizes  $\Delta V$  consumption while maintaining mission and safety constraints for both long-term station-keeping and rapid scatter and regather. The software seamlessly integrates functionality for both within a consolidated guidance and control system by adapting a robust simulated annealing heuristic search algorithm with an underlying linear programming impulsive burn solver. The maneuver planning software can account for initial, final, and interior state constraints while also minimizing  $\Delta V$  consumption. In addition to station-keeping and reconfiguration operations, the algorithms enable the rapid scatter and regather of the cluster modules. In order to rapidly execute scatter within the relatively short time window, the application maintains a set of pre-computed scatter maneuver plans that may be retrieved and quickly corrected to account for the latest navigation state estimates. The performance of the algorithms is demonstrated in terms of the module trajectories,  $\Delta V$ , inter-module distances, and relative orbit elements for several cases including four, twelve and twenty module clusters and both a nominal full scatter scenario as well as a scaled down scatter scenario.*

**Keywords:** *DARPA System F6, Proximity Operations, Relative Motion, Cluster Flight, Formation Flying, Scatter, Regather.*

### 1. Introduction

The Defense Advanced Research Projects Agency (DARPA) System F6 (Future, Fast, Flexible, Fractionated, Free-Flying Spacecraft United by Information Exchange) program seeks to address the challenge of developing future space systems via fractionated architectures wherein a network of spacecraft communicate, collaborate and share resources to accomplish their mission [1]. During nominal orbit operations, the spacecraft would maintain a loose cluster formation through station-keeping and reconfiguration maneuvers.

One of the objectives of the System F6 program was to demonstrate the capability to scatter the clustered spacecraft to rapidly evade a debris-like threat and then regather the scattered spacecraft into a re-formed cluster. It was required that within 5 minutes after a scatter command was received from the ground, the spacecraft disperse from their initial positions such that each spacecraft would be at least 10 km from where any spacecraft would have been under normal orbit operations. The planning and execution of the scatter and regather maneuvers would be performed autonomously without intervention or communication from ground operators.

Emergent Space Technologies has developed robust and scalable cluster flight guidance, navigation, and control (GN&C) simulation software called Cluster Flight Application (CFA) [2]. The guidance and control algorithms of CFA optimize  $\Delta V$  consumption while maintaining mission and state constraints for both long-term station-keeping and rapid scatter, seamlessly integrating functionality for both within a consolidated guidance and control system. These unique use cases are achieved through a robust simulated annealing heuristic search algorithm with an underlying linear programming impulsive burn solver. The maneuver planning software can account for initial, final, and interior state constraints while also minimizing  $\Delta V$  consumption.

This paper focuses on the scatter and regather strategies that were implemented and tested for System F6. In order to rapidly execute scatter within the relatively short time window, CFA maintains a database of pre-computed scatter maneuver plans that may be retrieved and quickly corrected to account for the latest cluster configuration. The correction operations are conducted independently on-board each spacecraft using computationally-fast algorithms that help to minimize the delay between reception of the scatter command and maneuver execution. During the generation of the pre-computed scatter maneuver plans, the  $\Delta V$  is minimized across the scatter and regather maneuvers through a set of optimized target hold orbits. The hold orbits serve as a staging point for subsequent ingress maneuvers to re-form the cluster into its nominal final configuration.

## 1.1. Nomenclature

This paper adopts the nomenclature used in DARPA's System F6 program and the original Broad Agency Announcement (BAA) [3]. Definitions for some of the key terms and concepts are listed below.

- Cluster: A set of spacecraft with nearly equal orbital elements able to maintain a stable relative geometry to support wireless communications. There is no requirement for precision relative station-keeping such as might be needed for formations performing coherent sensing or synthesizing sparse apertures. [3]
- Module: An independent spacecraft that is part of a fractionated cluster and cluster network, and that makes one or more of its components available as shared resources on the cluster network. [3]
- Cluster Configuration: A set of relative orbit elements (ROEs) or relative positions and velocities for each of the modules in the cluster relative to a common reference orbit, which may or may not coincide with an actual module.
- Cluster Reference Orbit: A common reference orbit defined in terms of instantaneous orbital elements or position and velocity and used as a reference orbit relative to which the cluster configuration is defined.
- Passive Safety: Low probability of collision even if there is a total loss of control.

## 1.2. Scatter and Regather Scenario

The original DARPA System F6 BAA dictated the following requirements for scatter and regather:

“Capability to perform a defensive cluster scatter and regather maneuver to rapidly evade a debris-like threat; specifically, 5 minutes after a command is received from the ground, each module should be at least 10 km from where any module would have been under normal orbit operations (i.e., if no scatter maneuver had been initiated)” [3]

and

“the ability to perform multi-body cluster flight with reasonable propellant optimality, a high level of assurance that trajectories are passively safe or safe to most probable on-orbit failure modes, and simultaneous capability for rapid maneuver planning as needed for a defensive scatter maneuver”[3]

As captured in these BAA requirements, the scatter and regather scenario occurs in response to a ground command for evading a debris-like object threatening to collide with the nominal trajectories of the modules. The modules should respond to the scatter command with minimal delay by performing a coordinated evacuation from their nominal trajectories and reconvening at a new cluster orbit location. This is depicted in Figure 1 for a four module cluster.

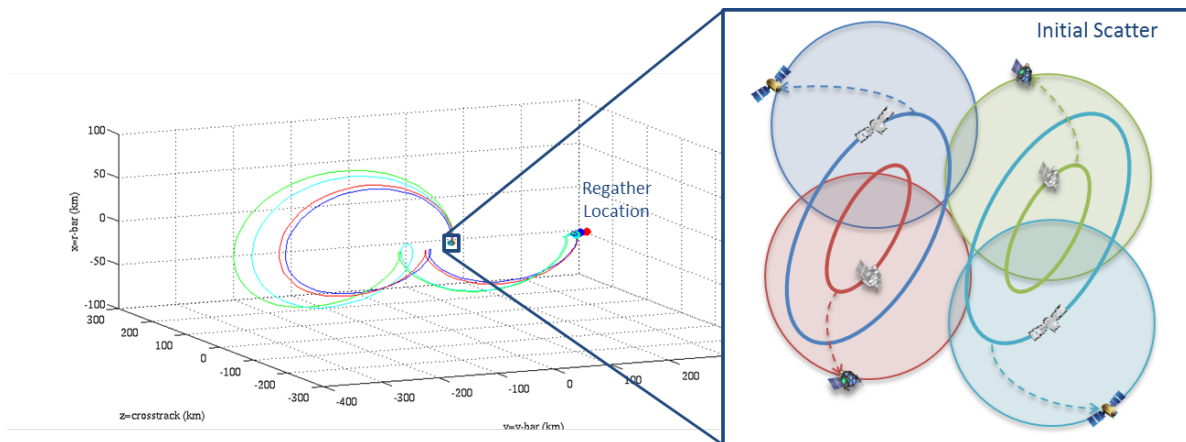


**Figure 1: Notional Scatter and Regather Trajectories for a Four Module Cluster**

While the initial scatter requirements are fairly explicit, the post-scatter and regather requirements are comparably open-ended. To maximize the system flexibility and optimize the system performance, Emergent developed an integrated three stage approach to the scatter and regather operations: initial scatter from the nominal trajectories, scattering to a set of intermediary hold orbits, and regathering the modules into a nominal cluster configuration. While each phase is characterized and influenced by different dynamical constraints and operational requirements, they are not computed independently. Rather, CFA computes the maneuvers required in a coordinated manner in order to minimize the total  $\Delta V$  across all three phases. CFA also ensures that operational and passive safety constraints are maintained across all three phases.

The initial scatter phase consists of maneuvers to rapidly disperse the modules from their nominal trajectories within a finite window of time and to a specified minimum distance. The requirements dictated that within 5 minutes after a scatter command was received from the ground, the spacecraft

modules would scatter to a minimum separation distance of 10 km from the nominal spacecraft trajectories. In other words, within 5 minutes of the scatter command, the spacecraft modules must be at least 10 km away from where any spacecraft would have been had the scatter command not been issued.

Following the initial scatter, the modules must perform a series of maneuvers to relocate the cluster around a new cluster reference orbit location. The new location is configurable, but typically includes some down-range separation from the original location as in the case depicted in Figure 1. It may also include radial and/or cross-track separations or no separation if the desire is to return back to the initial cluster location following scatter. Since there was no explicit requirement regarding the final regather location, the system must be capable of handling a range of possible regather locations while continually maintaining operational and passive safety constraints and minimizing the fuel consumption. To achieve this flexibility, Emergent developed the concept of the hold orbits to serve as a set of waypoints connecting the scatter and regather phases. They are not explicitly required, but as configurable parameters they serve as a useful method for designing scatter operations and minimizing the  $\Delta V$  required while accounting for the final regather configuration. Further details regarding the hold orbit design is discussed in Section 2.1.2.

By incorporating the concept of hold orbits, the system has the capability to perform scatter and regather in unison or as distinct phases. Scatter and regather operate in unison if the hold orbit targets are configured to match the final cluster configuration. Otherwise, the regather phase consists of a series of module ingresses from the hold orbits to the nominal cluster configuration as depicted in Figure 2. In this manner, the incorporation of hold orbits generates both performance flexibility in minimizing the total  $\Delta V$  relative to the hold orbit search space as well as operational flexibility in how and when to execute the regather maneuvers. The scalable and adaptable hold orbit search space also provides the ability to target a configuration with a low probability of collision ( $P_c$ ) in consideration of module thruster error and potential loss of communication or control. The regather ingress maneuvers can occur autonomously or in response to a separate regather command and in either case are optimized to reduce the total  $\Delta V$  required while maintaining the operational and passive safety constraints. Typically the ingresses occur one module at a time, but simultaneous ingresses are also feasible.

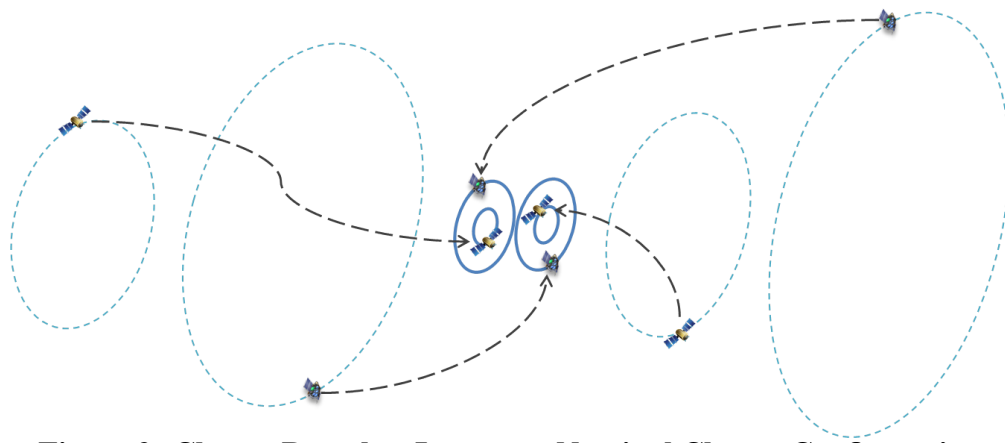


**Figure 2: Cluster Regather Ingress to Nominal Cluster Configuration**

### 1.3. Emergent Cluster Flight Application

To achieve the goals of the System F6 Cluster Flight technical area, Emergent developed service-based GN&C flight simulation software called the Cluster Flight Application (CFA). CFA incorporates cluster flight services that communicate using wireless messaging between modules to provide GN&C services and execute the mission use cases [2]. A single instance of the Cluster Flight Manager (CFM) resides on a single cluster module with possible back-ups present on other modules. Instances of the Navigation service (NAV) and Module Maneuvering Service (MMS) exist on each module within the cluster. The Orbit Maintenance Service (OMS) and Maneuver Planning Service (MPS) each need at least one instantiation either on a module or on the ground, but in some cases having multiple instances for these services may be beneficial for parallel processing or redundancy.

Figure 3 shows the interaction between the various services. CFM serves as the main hub for passing data and messages between the other services. Each instance of NAV processes Global Positioning System (GPS) data and relative range measurements through an extended Kalman filter to generate real-time state and covariance updates. These are provided to CFM, which maintains an inventory of the module states and characteristics. OMS houses the guidance algorithms for monitoring the cluster states and Pc and determining whether maneuver planning is required. If so, OMS interacts with MPS to generate a set of maneuvers and provides those back to CFM. CFM then distributes the maneuvers to each module's MMS for processing and execution using the on-board propulsion system. With this design architecture, CFA is capable of providing GN&C services to the cluster while sharing resources across the cluster modules and the ground.

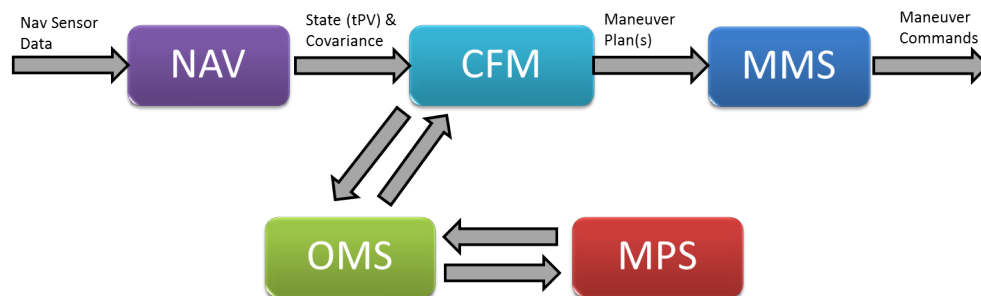


**Figure 3: Service-Based Cluster Flight Application**

### 1.4. Orbit Maintenance and Maneuver Planning for Scatter and Regather

The orbit maintenance and maneuver planning services depicted in Figure 3 provide the core guidance and control (G&C) algorithms for CFA. OMS primarily serves to monitor the cluster Pc and also to determine if any modules have drifted far enough from their nominal trajectories to warrant new maneuver plans. The degree of drift is measured relative to a set of control boxes formulated around the nominal module trajectories and the evolving mission objectives for station-keeping, cluster reconfiguration and scatter/regather. If OMS determines the modules require maneuvering, it provides a set of target orbits and other supporting data to MPS, which contains the necessary

algorithms to compute the required maneuver plans. More details regarding the closed-loop monitoring services provided in OMS and the algorithms used in MPS are available in separate technical papers [4, 5].

A key advantage of CFA is the incorporation of a consolidated set of core G&C algorithms that can robustly handle a wide range of use cases from station-keeping to scatter and regather. In particular, the MPS algorithms can solve both two-point boundary value problems as well as multi-point boundary value problems with interior state constraints [4]. Furthermore, in both cases, it uses the same set of algorithms and provides a reasonable balance between generating accurate solutions and doing so in a computationally expedient manner. The primary components in MPS are depicted in Figure 4. At the deepest level, it uses an impulsive multi-burn solver and linear programming (LP) to compute a set of maneuvers for a given boundary value problem. The burn solver is embedded within a heuristic search engine based on simulated annealing (SA) that determines the best operationally feasible solution within a discretized search space. The primary objective for the scatter and regather problem is to minimize the  $\Delta V$  while satisfying the scatter constraints, maximum per-module  $\Delta V$  limits, maximum and minimum inter-module distances (IMDs) and other operational constraints.

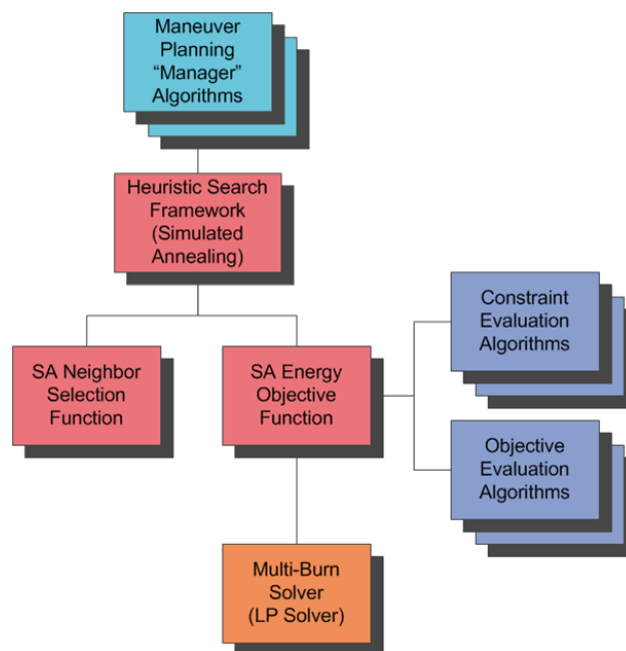


**Figure 4: Maneuver Planning Service**

## 2. Enabling Technologies for Scatter and Regather

### 2.1. Driving Requirements

The primary DARPA and system design requirements for scatter and regather were discussed in Section 1. Additional driving requirements were identified through analysis and system trade studies. These include propulsion thrust requirements and the design of the hold orbits.

### 2.1.1. Thrust Requirements

Among the key aspects dictated in the requirements, the 10 km in 5 minutes most directly influences the necessary performance for CFA in achieving the scatter and regather scenario. It also strongly influences the necessary propulsion system, which must have sufficient thrust capacity to achieve this constraint. As a rough illustration, the straight-line kinematics for varying constant-thrust profiles are shown in Figure 5 for a corresponding mass of 180 kg.

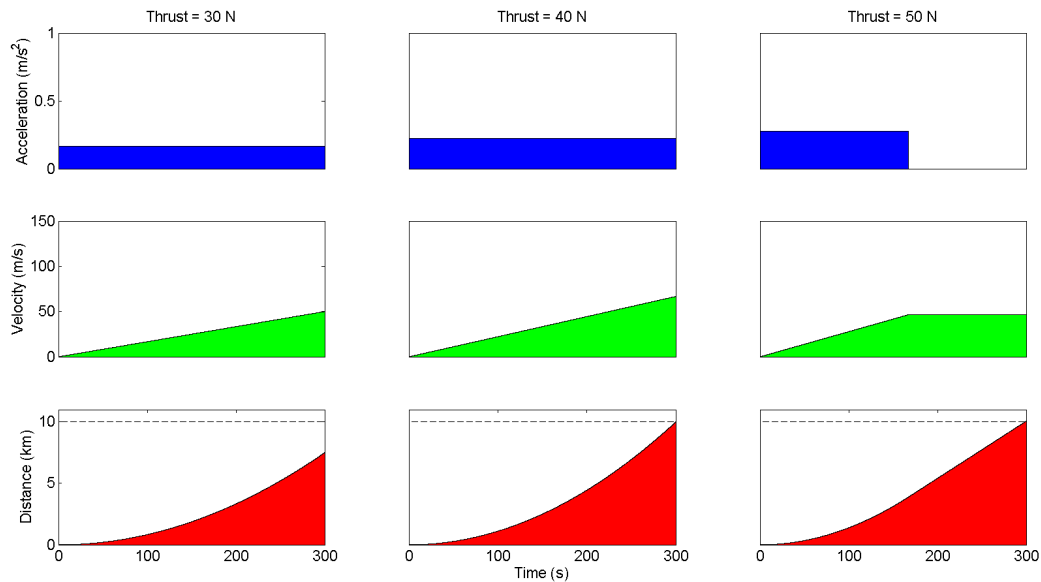


**Figure 5: Constant-Acceleration Kinematics for varying Thrust Levels**

While the 40 N and 50 N propulsion systems can achieve the minimum 10 km in 5 minutes constraint, the 30 N propulsion system cannot. Further, the 50 N propulsion system can achieve the 10 km distance in less time than the 40 N system or using less  $\Delta V$  as depicted in Figure 5. This provides a rough estimate of the minimum required thrust capacity for the propulsion system in order to achieve the scatter objectives. Of course, the actual minimum thrust required is subject to the full system dynamics and perturbations and can be higher if the spacecraft slew time and propulsion preparation time have to be included within the 5 minute constraint window. Other mission objectives and considerations also affect the propulsion system design including station-keeping performance [5], thruster errors, and system response times, among others.

### 2.1.2. Regather Targeting

As discussed in Section 1, the modules can scatter and immediately regather back to the initial conditions or incorporate a change in the cluster reference orbit location (such as down-range or with a change in altitude). The CFA G&C system is capable of targeting a wide variety of regather orbits and generating maneuvers with reasonable fuel optimality through the inclusion of a set of intermediary hold orbits between the scatter and regather phases. The hold orbits are centered around the final cluster configuration targets, but with two layers of buffers: one for passive safety

and one to expand the target orbits into a target search space within which MPS can optimize the regather maneuvers. The regather hold orbit search space is depicted in Figure 6.

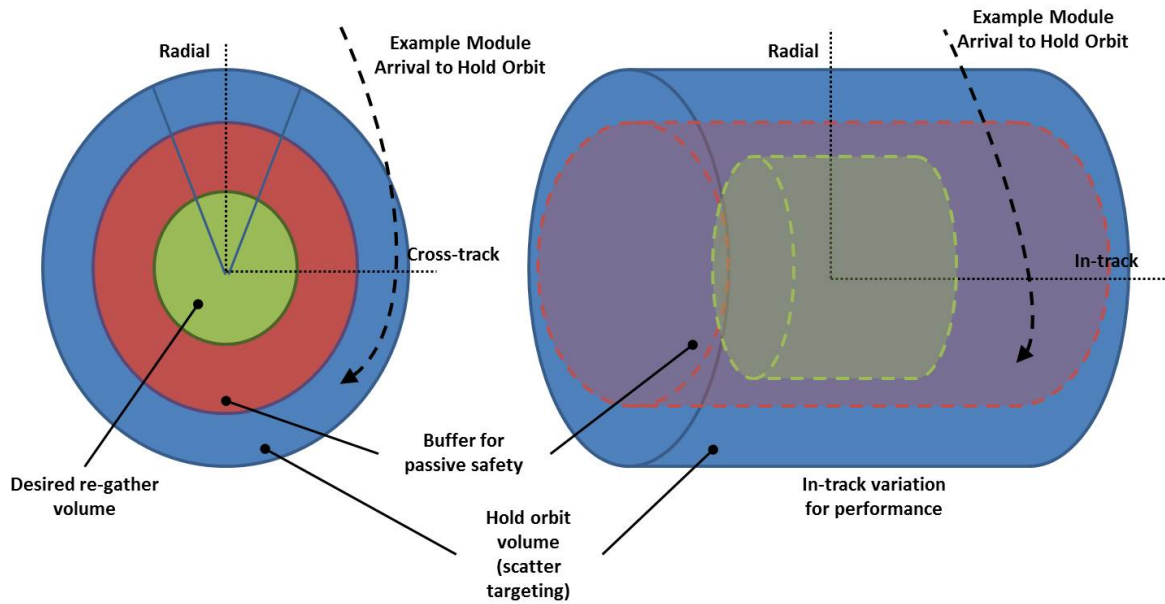


**Figure 6: Regather Targeting using Hold Orbits**

The target orbits and hold orbit search space are defined in terms of relative orbit elements (ROEs) [6, 7, 8]. The ROEs comprise a set of state variables  $[a_e, x_d, y_d, \beta, z_{max}, \gamma]$  in the spirit of the classical orbital elements that together describe the size, shape and orientation of a module orbit around the reference point as well as its location within the relative orbit. The in-plane ROEs of  $a_e, x_d, y_d$ , and the in-plane phase angle  $\beta$  are shown in Figure 7 while the remaining elements of  $z_{max}$  and  $\gamma$  represent the maximum cross-track displacement and cross-track phase angle respectively.

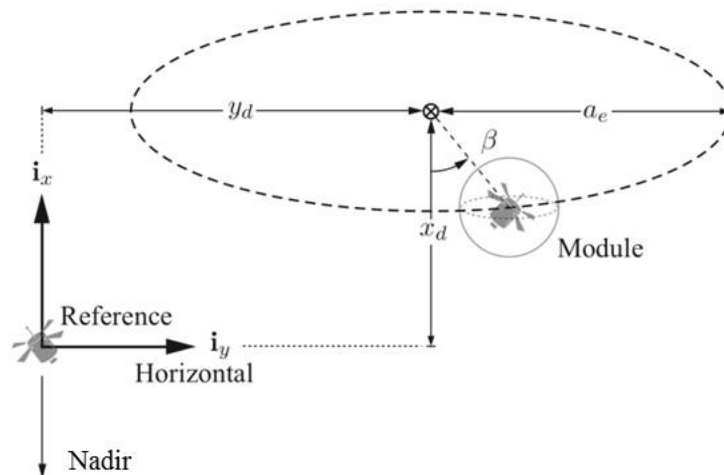


**Figure 7: In-Plane Relative Orbit Elements**

The hold orbit search space is defined by Eq. 1 where target subscripts denote the nominal final cluster configuration ROEs and buffer, max scale and range limit subscripts are all configurable parameters for scaling the hold orbit ranges depicted in Figure 6.

$$\begin{aligned}
 a_e \in & \left[ \begin{array}{l} (a_{e,target} + |x_{d,target}|) + a_{e,buffer} \quad a_{e,maxscale}(a_{e,target} + |x_{d,target}|) + a_{e,buffer} \end{array} \right] \\
 x_d \in & \left[ \begin{array}{l} -x_{d,rangelimit} \quad x_{d,rangelimit} \end{array} \right] \\
 y_d \in & \left[ \begin{array}{l} y_{d,target} - y_{d,rangelimit} \quad y_{d,target} + y_{d,rangelimit} \end{array} \right] \\
 \beta \in & \left[ \begin{array}{l} \beta_{target} - \beta_{rangelimit} \quad \beta_{target} + \beta_{rangelimit} \end{array} \right] \\
 z_{max} \in & \left[ \begin{array}{l} z_{max,target} + z_{max,buffer} \quad z_{max,scale}(z_{max,target}) + z_{max,buffer} \end{array} \right] \\
 \gamma \in & \left[ \begin{array}{l} \gamma_{target} - \gamma_{rangelimit} \quad \gamma_{target} + \gamma_{rangelimit} \end{array} \right]
 \end{aligned} \tag{1}$$

Note that the  $a_e$  range is formulated in order to maintain passive safety between the hold orbits and final regather configuration. Incorporating the hold orbit ROE ranges, MPS has a constrained final state space within which it can search for near-optimal post-scatter and regather maneuver plans. In addition, the configurability of the parameters included in Eq. 1 provide the flexibility for the ground to tune the configurable parameters in order to improve performance or enforce any additional operational constraints such as fixing the module phase angles (zero  $\beta$  and  $\gamma$  limits) or increasing the passive safety buffers.

## 2.2. Enforcing Scatter Constraints in the CFA Maneuver Planning Service

For normal operations of station-keeping and reconfiguration, the two-point boundary value problem serves as a sufficient formulation to generate maneuver plans for closed-loop orbit maintenance. However, scatter and regather present the challenging aspect of constraining the solution space within a non-convex state space. The scatter constraint imposes a time-tagged interior constraint (5-minutes past scatter) for which the module position is a minimum distance (10 km) away from its corresponding un-scattered position.

In addition to the explicit time-tagged interior constraint, the scatter and regather scenario also incorporates the concept of the keep-out zones (KOZs) that are continually enforced throughout the scatter and regather duration. The KOZs are initialized by the time-tagged interior constraint as a sphere surrounding each of the module positions at the interior constraint time (5 minutes past scatter). The KOZs are propagated in parallel with the original (pre-scatter) module trajectories and enforced as exclusion regions throughout the scatter phase. The propagated KOZs are depicted in Figure 8.

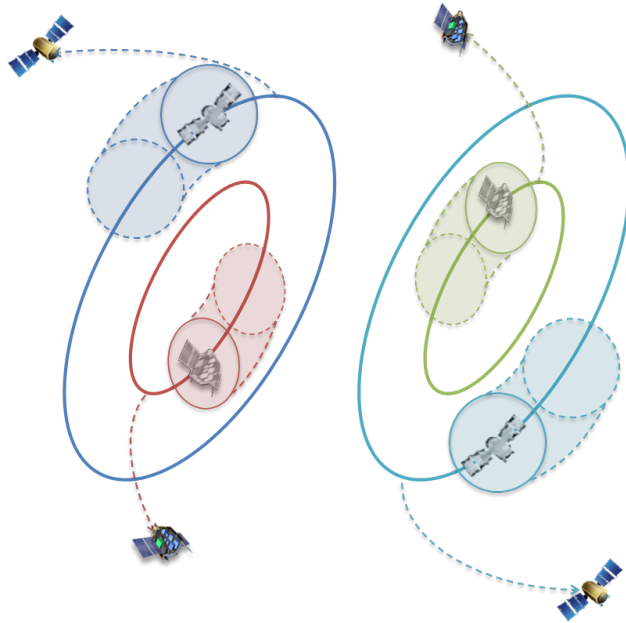


**Figure 8: Propagated Scatter Keep-Out Zones**

### 2.2.1. Keep-Out Zones in the CFA Heuristic Search Algorithm

The CFA heuristic maneuver planning search algorithm is designed using Simulated Annealing. The algorithm searches across a discretized search space for the best solution for module maneuver plans as generated by the embedded burn solver. The best solution is measured in terms of its “energy”, which represents the modules’  $\Delta V$  and the satisfaction of the mission constraints for the inter-module distances (IMDs), burn size limits, and KOZs. The constraints and minimum- $\Delta V$  objective are independently weighted for focused performance tuning. The search algorithm design is discussed in greater detail in a separate technical paper [4]. A notional search profile is illustrated in Figure 9.

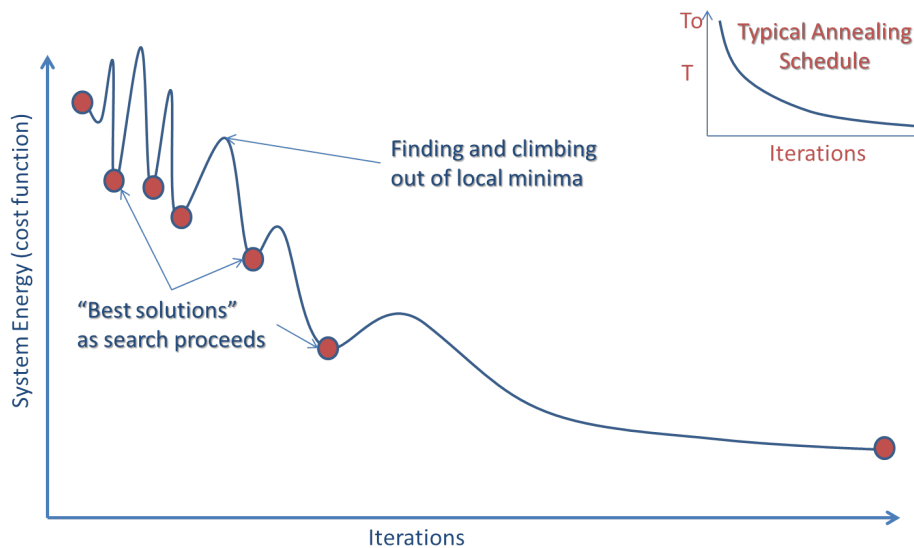


**Figure 9: Notional Search Profile for the Heuristic Search Algorithm**

The scatter KOZ constraints are weighted both in terms of the boolean violation of the exclusion regions as well as by the normalized distance from the center of the KOZs. In this manner, the SA algorithm can formulate KOZs as both binary and smooth energy constraints.

### 2.2.2. Multi-Point Boundary Value Problem in the CFA Burn Solver

The burn solver can enforce both inequality and equality interior constraints. For the purposes of scatter, the scatter target is enforced as interior equality state constraints as generated by an explicit position target on or above the initial KOZ surface. The SA algorithm provides these target positions by discretizing the KOZ surface around its center in terms of altitude (above the surface) and azimuth and elevation angles. It then incorporates these parameters into the global search space.

The burn solver solves the multi-point boundary value problem by linearizing the system dynamics and formulating the transfer problem as a linear program (LP). The system dynamics and ROE targets are recomputed relative to a target reference orbit generated from propagating the final state target backward to the initial time. This is represented in Figure 10 where the red dotted curve represents the cluster reference orbit, the green dashed curve represents the backward propagated target reference orbit, the blue solid curve and stars represent the computed maneuver trajectory and notional maneuvers respectively. Using the backward propagated target reference orbit in place of the cluster reference orbit provides better accuracy due to the smaller scale of the relative variations.

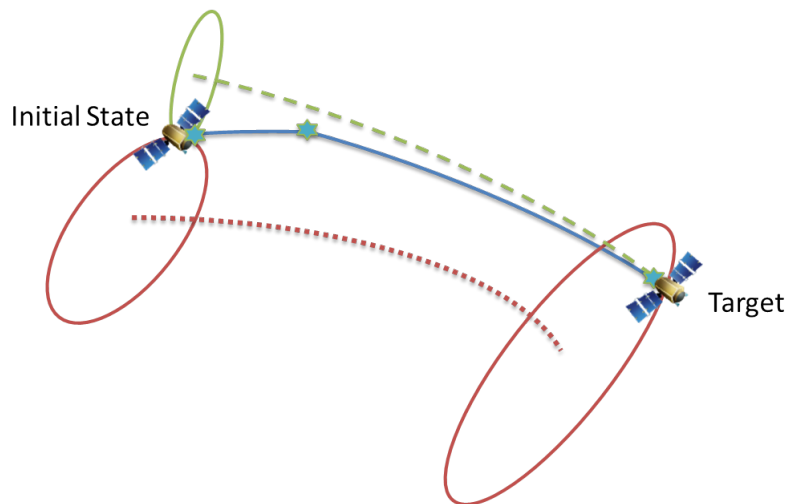


**Figure 10: Recomputing the Target Reference Orbit**

The relative system dynamics are linearized about the target reference orbit using the geometric model developed by Gim and Alfriend [9, 10, 11], which incorporates eccentricity and first-order  $J_2$  perturbations. The geometric model provides an analytical, linearized approximation of the dynamical state transition matrix mapping variations in the state at different points in time. This is represented in Eq. 2 where  $\phi_{f,0}$  maps between variations in the initial state  $[\vec{r}(t_0) \quad \vec{v}(t_0)]^T$  to

corresponding variations in the final state  $[\vec{r}(t_f) \quad \vec{v}(t_f)]^T$ .

$$\begin{bmatrix} \delta\vec{r}_f(t) \\ \delta\vec{v}_f(t) \end{bmatrix} = \phi(t_f, t_0) \begin{bmatrix} \delta\vec{r}(t_0) \\ \delta\vec{v}(t_0) \end{bmatrix} = \phi_{f,0} \begin{bmatrix} \delta\vec{r}(t_0) \\ \delta\vec{v}(t_0) \end{bmatrix} = \begin{bmatrix} A_{f,0} & B_{f,0} \\ C_{f,0} & D_{f,0} \end{bmatrix} \begin{bmatrix} \delta\vec{r}(t_0) \\ \delta\vec{v}(t_0) \end{bmatrix} \quad (2)$$

Adopting a similar methodology as used in Tillerson, Inalhan and How [12], an analytical approximation for the pulse response of the system due to a series of impulsive maneuvers  $\vec{u}_i = \Delta\vec{V}_i$  is derived by applying the state transition matrix between each neighboring pair of maneuvers. Partitioning the state transition matrix as shown in Eq. 2, the cumulative system response for the variation in the final state after  $N$  impulsive maneuvers is given by Eqs. 3-5.

$$\phi_{N,k} = \begin{cases} \prod_{i=k}^{N-1} \phi_{i+1,i} & \text{for } 0 \leq k < N \\ I_6 & \text{if } k = N \end{cases} \quad (3)$$

$$\delta\vec{r}_N = \sum_{j=0}^{N-1} \left( \prod_{i=j+1}^{N-1} A_{i+1,i} \right) B_{j+1,j} \vec{u}_j \quad (4)$$

$$\delta\vec{v}_N = \vec{u}_N + \sum_{j=0}^{N-1} \left( \prod_{i=j+1}^{N-1} C_{i+1,i} \right) D_{j+1,j} \vec{u}_j \quad (5)$$

Incorporating state constraints and decomposing the control into positive and negative parts  $\vec{u}_i = \vec{u}_i^{(+)} - \vec{u}_i^{(-)}$ , the system pulse response is reformulated into the LP problem:

- Minimize the  $L^1$ -norm of the impulse vectors

$$\min \sum_{i=0}^N |\vec{u}_i| = \min \sum_{i=0}^N \left( |\vec{u}_i^{(+)}| + |\vec{u}_i^{(-)}| \right) \quad (6)$$

- Subject to the linearized dynamics in Eqs. 4 and 5, the control constraints

$$\begin{aligned} \vec{u}_i^{(+)} &\geq 0 \\ \vec{u}_i^{(-)} &\geq 0 \end{aligned} \quad \text{for } i = 1 : N \quad (7)$$

boundary value constraints

$$\begin{aligned} \vec{r}_0 &= \vec{r}_{\text{init}} \\ \vec{v}_0 &= \vec{v}_{\text{init}} \\ \vec{r}_N &= \vec{r}_{\text{target}} \\ \vec{v}_N &= \vec{v}_{\text{target}} \end{aligned} \quad (8)$$

and interior state constraints

$$\begin{aligned} \vec{r}_j &= \vec{r}_{\text{target},j} \\ \vec{v}_j &= \vec{v}_{\text{target},j} \end{aligned} \quad (9)$$

where  $j = 1 : M \subset [ 1 \quad N ]$  with  $M$  representing the number of interior constraints.

The resulting LP problem is solved using the revised simplex method [13, 14], which is a technique for the optimization of a linear objective function subject to linear equality and linear inequality constraints as in Eqs. 3 - 9. The LP solver finds the optimal solution to well formed LP problems that have a bounded solution, and it also detects infeasible problems, unbounded solutions and degenerate problems.

### 2.3. Pre-Planned Scatter Cluster Maneuver Plans

To enable rapid scatter execution, CFA pre-computes scatter maneuver plans (SMPs) and stores them for future execution. CFA maintains a repository of pre-planned SMPs, which can be quickly retrieved, updated and executed in response to a ground command to scatter. This avoids the computational delay associated with generating a SMP at the time of scatter execution.

All CFA maneuver plans (including SMPs) have their burns described as impulsive or finite inertial-hold maneuvers in an absolute timescale. The burns are organized within cluster maneuver plans (CMPs), which contain associated module maneuver plans (MMPs) all of which are tagged with unique identifiers. Each SMP is also tagged with a coordination time, which represents a future time of scatter execution. The pre-planned SMPs are generated ahead of time based on the expected nominal cluster configuration at the coordination time. CFA periodically examines the contents of the stored SMPs, discards any stale plans, and generates new plans as necessary as depicted in Figure 11.

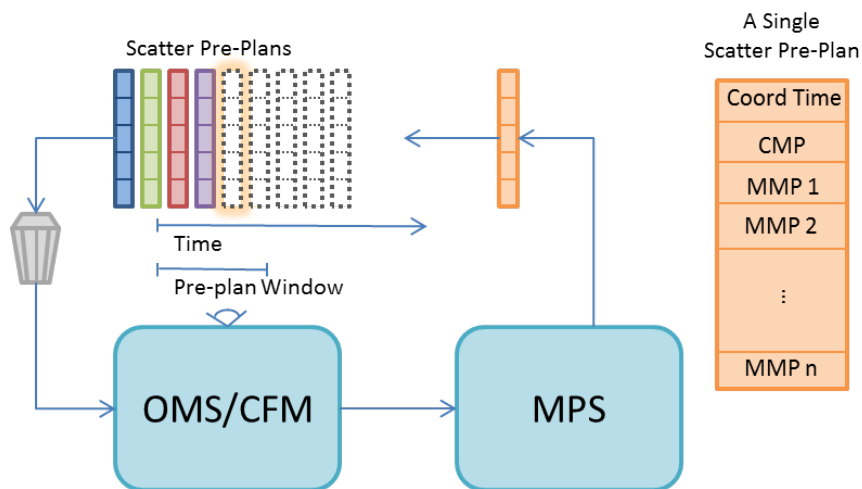


**Figure 11: Pre-Plan Scatter Computations**

The pre-computed SMPs are stored in time sequential order based on a set of configurable parameters including the time interval between each pre-plan, the maximum number of pre-plans, and the maximum pre-plan time window. CFA pre-computes SMPs up to either the maximum number of pre-plans or maximum time window depending on which occurs first. For example, an interval of 5 minutes between each pre-plan and a maximum of 25 pre-plans encompass a window of 125 minutes into the future. However, if the maximum time window is less than 125 minutes the pre-plans are only generated up to the maximum time. This provides the flexibility to tailor the storage and computation of SMPs.

The pre-planned SMPs are routinely checked, discarded and re-generated as necessary in response to changes to the cluster reference orbit or nominal cluster configuration. Since the pre-planned SMPs are computed based on the nominal cluster configuration, SMPs are agnostic to on-going station-keeping maneuvers and the relative drift between the modules. However, the performance of the executed SMP is affected by any discrepancies between the presumed cluster configuration and the actual cluster configuration at the time of execution. Performance errors occur due to the natural drift of modules away from the nominal configuration. This is mitigated by the station-keeping control tuning, which bounds the amount of drift permitted before executing correction maneuvers. Performance errors also arise from any difference in the pre-planned SMP coordination time and the actual time of scatter execution. The difference in time reflects a difference between the presumed cluster configuration and the actual cluster configuration at the time of execution. To mitigate this source of error, a correction algorithm adjusts the pre-planned maneuvers at the time of execution in order to account for the differences in the expected and actual cluster configuration. The adjustment is applied by a rotation of the maneuver  $\Delta V$  vectors within the local vertical curvilinear (LVC) frame. The degree of rotation is determined by the nominal module phase differences at the coordination time vs. the actual execution time. The correction algorithm also updates the associated maneuver and maneuver plan times to account for the true scatter execution time.

### 3. Analysis

#### 3.1. Scatter and Regather Performance

The results for a four module scatter simulation are shown in Figures 12 - 15. The cluster starts off in a nominal station-keeping configuration and the scatter command executes after approximately one orbit. The initial scatter burn disperses the cluster beyond the 10 km keep-out constraint within 5 minutes and the regather location is 200 km down-range. The scatter transfer time is configured at 3 orbits after which the modules perform station-keeping at the hold-orbits up to a total simulation duration of 10 orbits. The minimum IMD is maintained above 100 meters while a maximum IMD constraint is not enforced in this case. The final ROE targets are equal to the initial cluster configuration, which are used to generate the target hold orbit ranges as configured in Eq. 10.

$$\begin{aligned}
 a_e &\in \begin{bmatrix} (a_{e,target} + |x_{d,target}|) + 1000 & 2(a_{e,target} + |x_{d,target}|) + 1000 \\ y_{d,target} - 20,000 & y_{d,target} + 20,000 \\ z_{max,target} + 500 & 2(z_{max,target}) + 500 \end{bmatrix} \\
 y_d &\in \begin{bmatrix} \\ \\ \end{bmatrix} \\
 z_{max} &\in \begin{bmatrix} \\ \\ \end{bmatrix} \\
 x_d &= x_{d,target} \\
 \beta &= \beta_{target} \\
 \gamma &= \gamma_{target}
 \end{aligned} \tag{10}$$

While the final ROE targets are used to compute the hold orbit targets, the simulation results do not include the regather ingress maneuvers, but rather focuses on the scatter performance leading to hold orbit arrival. A demonstration of the regather ingress maneuvers is included in a separate technical paper [4]. The simulation generated pre-planned SMPs at 5-minute intervals and the executed plan had a time bias of 140 seconds, which was corrected through a rotation of the  $\Delta V$  vectors as discussed in Section 2.3.

The module trajectories are shown in Figure 12 including a 3-dimensional viewpoint as well as in radial/in-track and radial/cross-track planes. The modules initial scatter trajectories are similar in direction with a raise in the altitude in order to cycle the modules down-range. Small differences in the initial scatter directions and subsequent maneuvers result in diverging trajectories that ultimately re-converge to their respective hold orbits down-range from the initial cluster location.

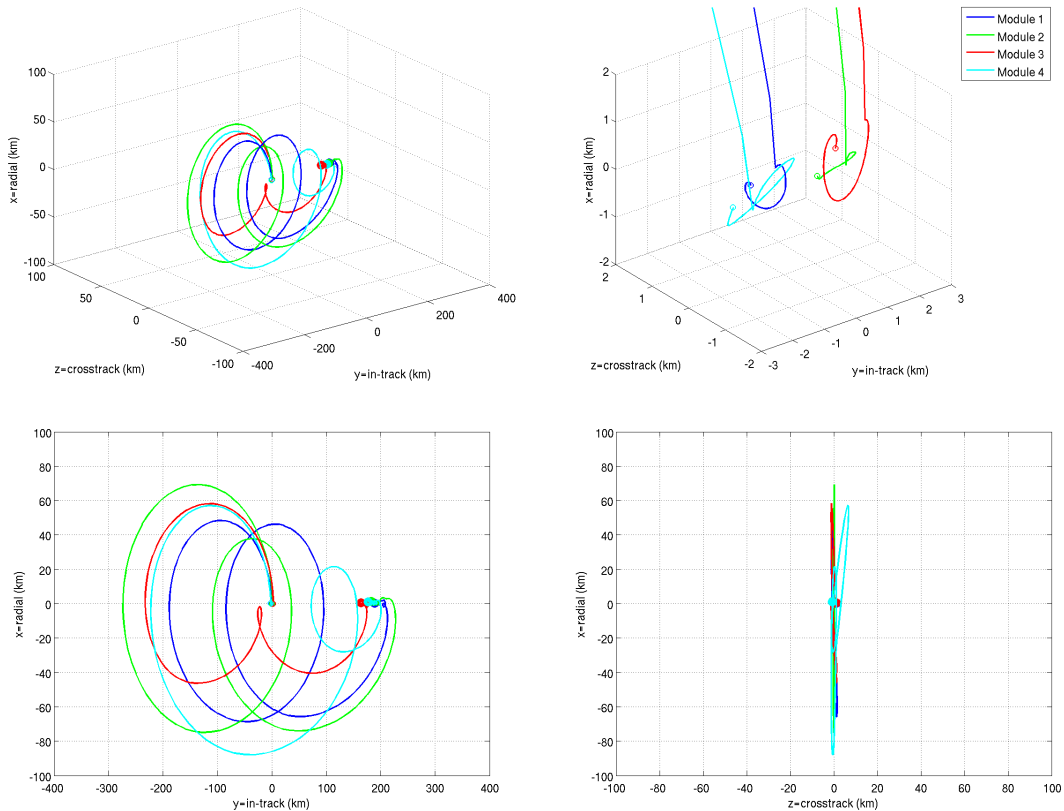


**Figure 12: Four Module Cluster Scatter Trajectories**

The module maneuver results are shown in Figures 13. The magnitudes of the initial scatter burn and subsequent maneuvers vary depending on the module location within the cluster configuration and the trajectories followed to achieve the re-formation. However, the general trend of the burn magnitudes are similar across the cluster. The average per module  $\Delta V$  is 70.6 m/s for the initial scatter burn, 39.7 m/s for the post-scatter burns, and 0.2 m/s for station-keeping at the hold orbits. The average per module total  $\Delta V$  is 110.5 m/s. Note that these results incorporate the full system dynamics and perturbations as well as buffers for system noise and system response and slew times. Thus, they are more reflective of the actual thrust requirements than those illustrated in the straight-line approximations discussed in Section 2.1.1.

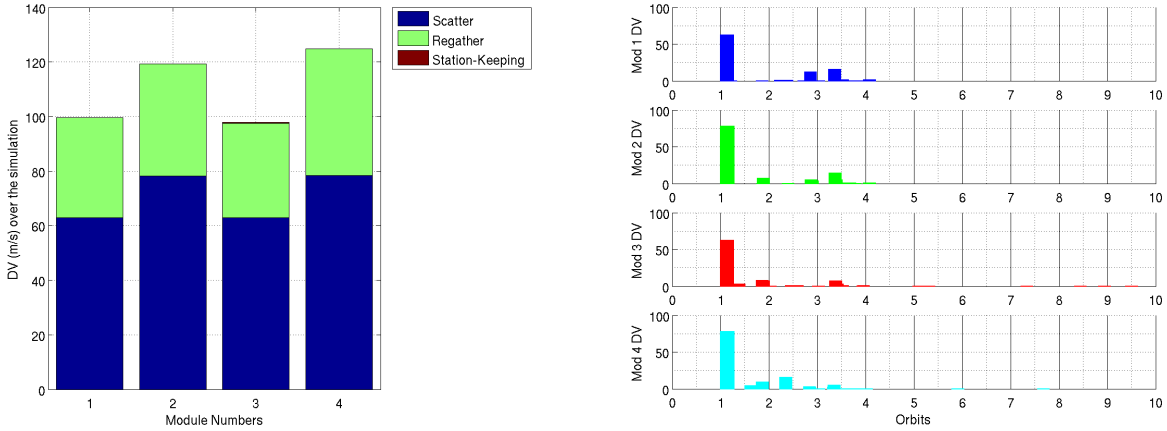


**Figure 13: Four Module Cluster Scatter Maneuvers**

The module trajectories are represented in terms of ROEs in Figure 14. The first subfigure depicts the module ROEs with respect to the initial cluster reference orbit, which is subsequently relocated 200 km downrange (expressed as  $y_d$  in terms of ROEs). The second subfigure depicts the non-angular module ROEs with respect to the initial cluster leader (Module 1), in order to demonstrate the results for the relative trajectories. The differences between the initial and final ROEs in the relative trajectories reflect the hold orbit buffers included in Eq. 10 and the expanded search space used by MPS to compute the best target hold orbits.

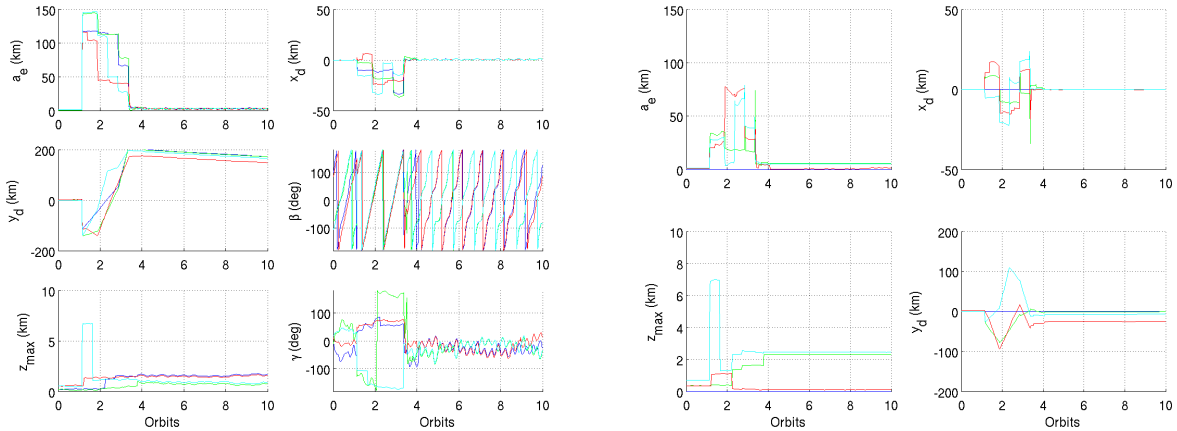


**Figure 14: Four Module Cluster Scatter ROEs with Respect to the Cluster Reference Orbit and the Leader Module**

The scatter performance results in terms of the IMDs and keep-out ranges are shown in Figure 15. The first subfigure shows the minimum IMD across the entire cluster, which stays above the configured threshold of 100 meters. It also shows the maximum IMD across the entire cluster, which is not constrained in this case, but nonetheless stays within 200 km, which is an acceptable range for inter-module communications. The second subfigure shows the keep-out ranges at 5 minutes after the scatter command. The keep-out ranges are given by the distance from each module to the center of each of the four keep-out zones (i.e. four modules and four KOZs for a

total of 16 keep-out ranges). All modules successfully achieve the minimum 10 km range from each keep-out zone.

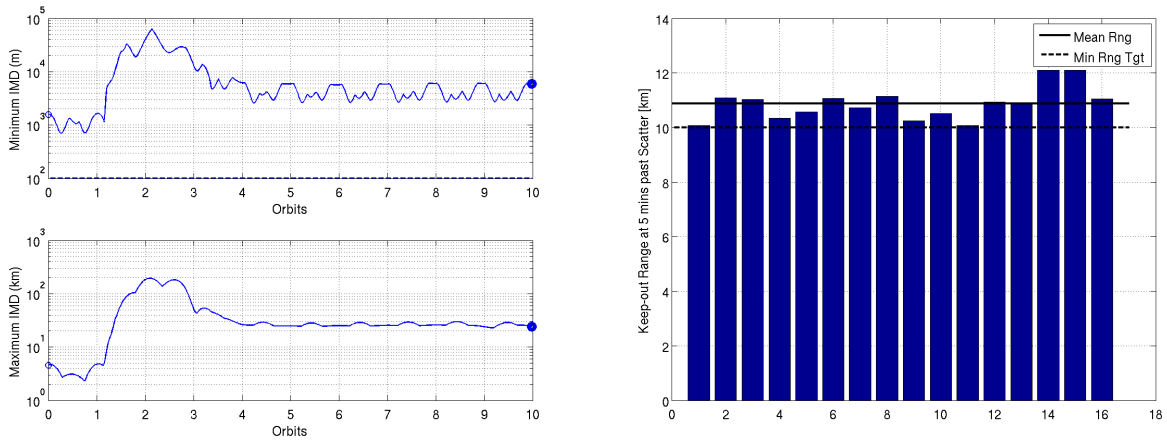


**Figure 15: Four Module Cluster Scatter Min and Max IMDs and Keep-Out Ranges**

### 3.2. Scalability

The CFA scatter and regather algorithms are scalable both in the number of modules and the size of the scatter distance. As a basis of comparison against the four module case presented in Section 3.1, the performance results for twelve and twenty module clusters are included in Sections 3.2.1-3.2.2 and a reduced scatter scenario is presented in Section 3.2.3.

#### 3.2.1. Twelve Module Scatter

The results for a twelve module scatter simulation are shown in Figures 16 - 19. The same configuration is used as in Section 3.1, but with 12 modules rather than 4. Since the pre-planning cycles were identical to the four module case, the executed plan again had a time bias of 140 seconds, which was corrected through a rotation of the  $\Delta V$  vectors as discussed in Section 2.3.

The module trajectories are shown in Figure 16 including a 3-dimensional viewpoint as well as in radial/in-track and radial/cross-track planes. The trajectories again exhibit significant changes in the altitude in order to cycle the modules down-range. With the higher number of modules, the initial scatter directions are more dispersed including one module that converged on a scatter trajectory in roughly the opposite direction from the others. All the modules successfully arrive down-range from the initial cluster location within the 3 orbit transfer time.

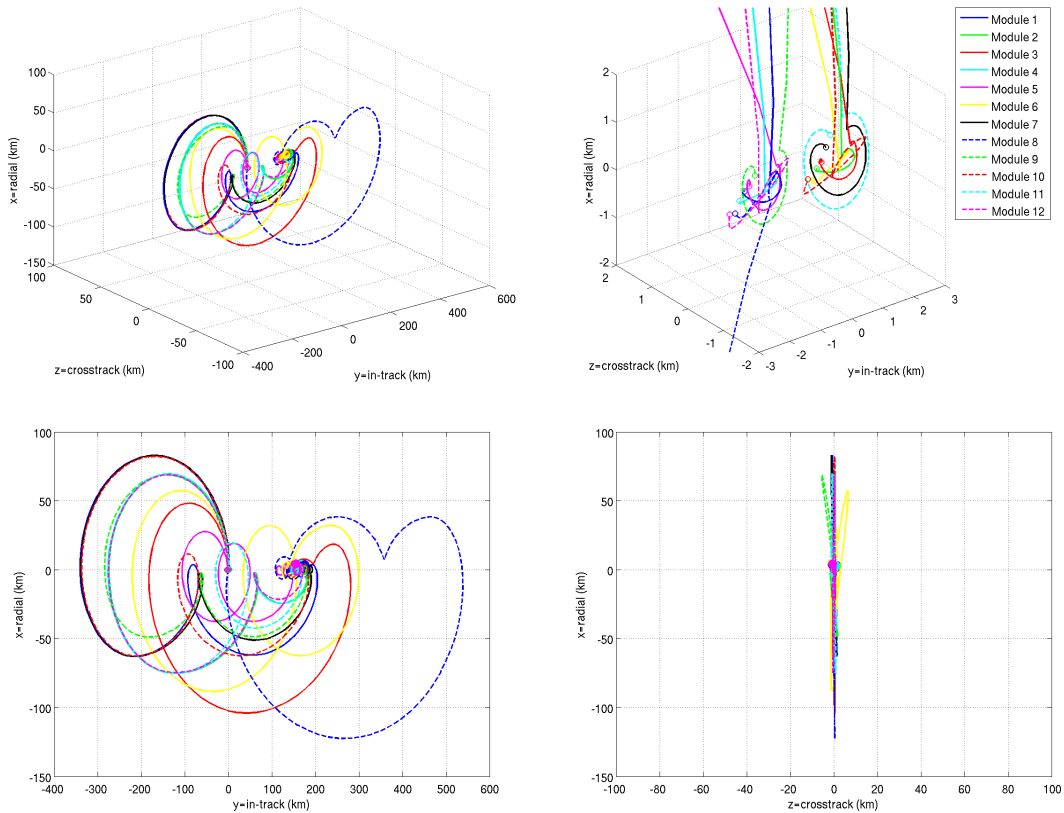


**Figure 16: Twelve Module Cluster Scatter Trajectories**

The module maneuver results are shown in Figure 17. The average per module  $\Delta V$  is 75.7 m/s for the initial scatter burn, 42.0 m/s for the post-scatter burns, and 2.5 m/s for station-keeping at the hold orbits. The average per module total  $\Delta V$  is 120.2 m/s. The  $\Delta V$  results are higher than in the four module case due to the added IMD and KOZ constraints enforced across the cluster.

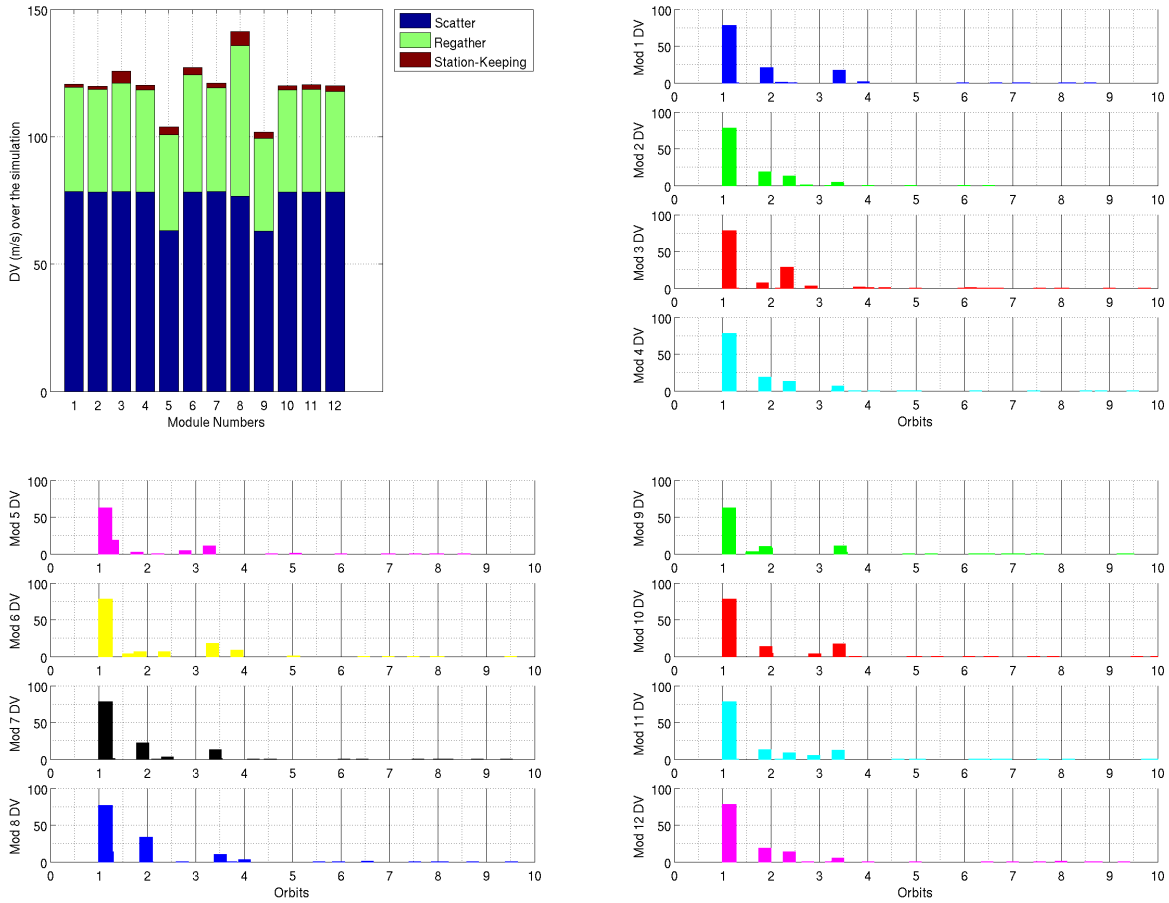


**Figure 17: Twelve Module Cluster Scatter Maneuvers**

The module trajectories are represented in terms of ROEs in Figure 18. The first subfigure depicts the module ROEs with respect to the initial cluster reference orbit, which is subsequently relocated 200 km downrange. The second subfigure depicts the non-angular module ROEs with respect to the initial cluster leader (Module 1), in order to demonstrate the results for the relative trajectories. The higher number of modules results in larger ROE displacements required to safely disperse the cluster and relocate them down-range at the target hold orbits.

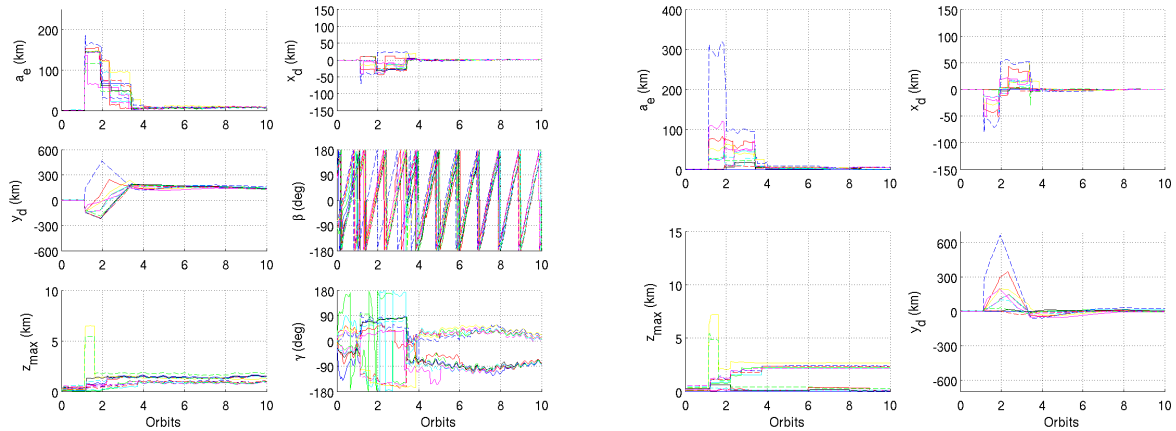


**Figure 18: Twelve Module Cluster Scatter ROEs with Respect to the Cluster Reference Orbit and the Leader Module**

The scatter performance results in terms of the IMDs and keep-out ranges are shown in Figure 19. The first subfigure shows the minimum IMD across the entire cluster, which stays above the configured threshold of 100 meters, as well as the maximum IMD. The minimum IMD gets smaller than the four module case since there are more modules flying within the space of the cluster. Conversely the maximum IMD is greater than the four module case since the modules take more dispersed paths during the post-scatter phase.

The second subfigure shows the keep-out ranges at 5 minutes after the scatter command. In this case there are 12 modules and 12 KOZs for a total of 144 keep-out range measurements. All modules successfully achieve the minimum 10 km range from each keep-out zone at 5 minutes past scatter.

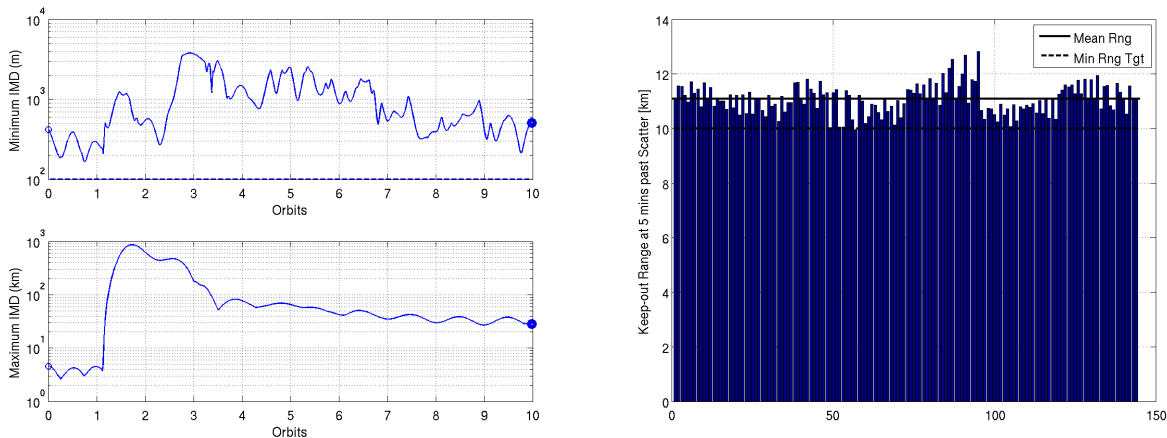


**Figure 19: Twelve Module Cluster Scatter Min and Max IMDs and Keep-Out Ranges**

### 3.2.2. Twenty Module Scatter

The results for a twenty module scatter simulation are shown in Figures 20 - 23. The same configuration is used as in Section 3.1, but with 20 modules rather than 4. Since the pre-planning cycles were identical to the four module case, the executed plan again had a time bias of 140 seconds, which was corrected through a rotation of the  $\Delta V$  vectors as discussed in Section 2.3.

The module trajectories are shown in Figure 20 including a 3-dimensional viewpoint as well as in radial/in-track and radial/cross-track planes. The trajectories again exhibit significant changes in the altitude in order to cycle the modules down-range. With the higher number of modules, the initial scatter directions are much more dispersed with modules both lowering and raising their altitudes in response to the scatter command. All the modules successfully arrive down-range from the initial cluster location within 3 orbits.

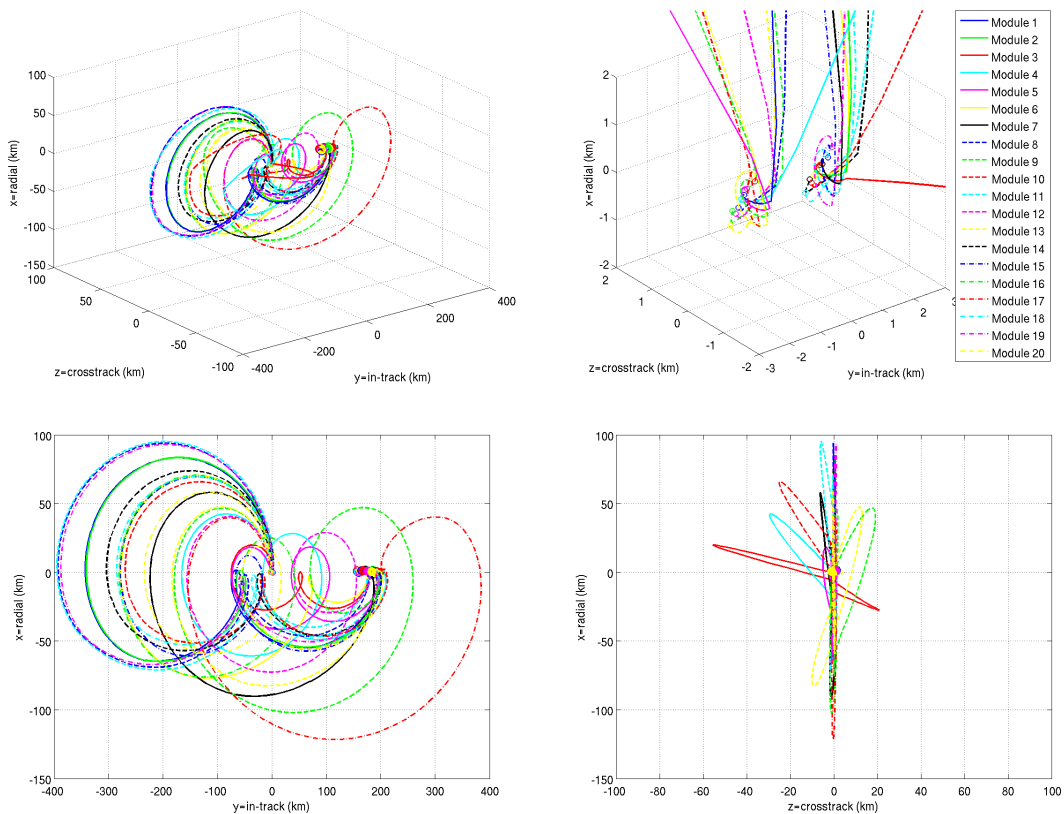
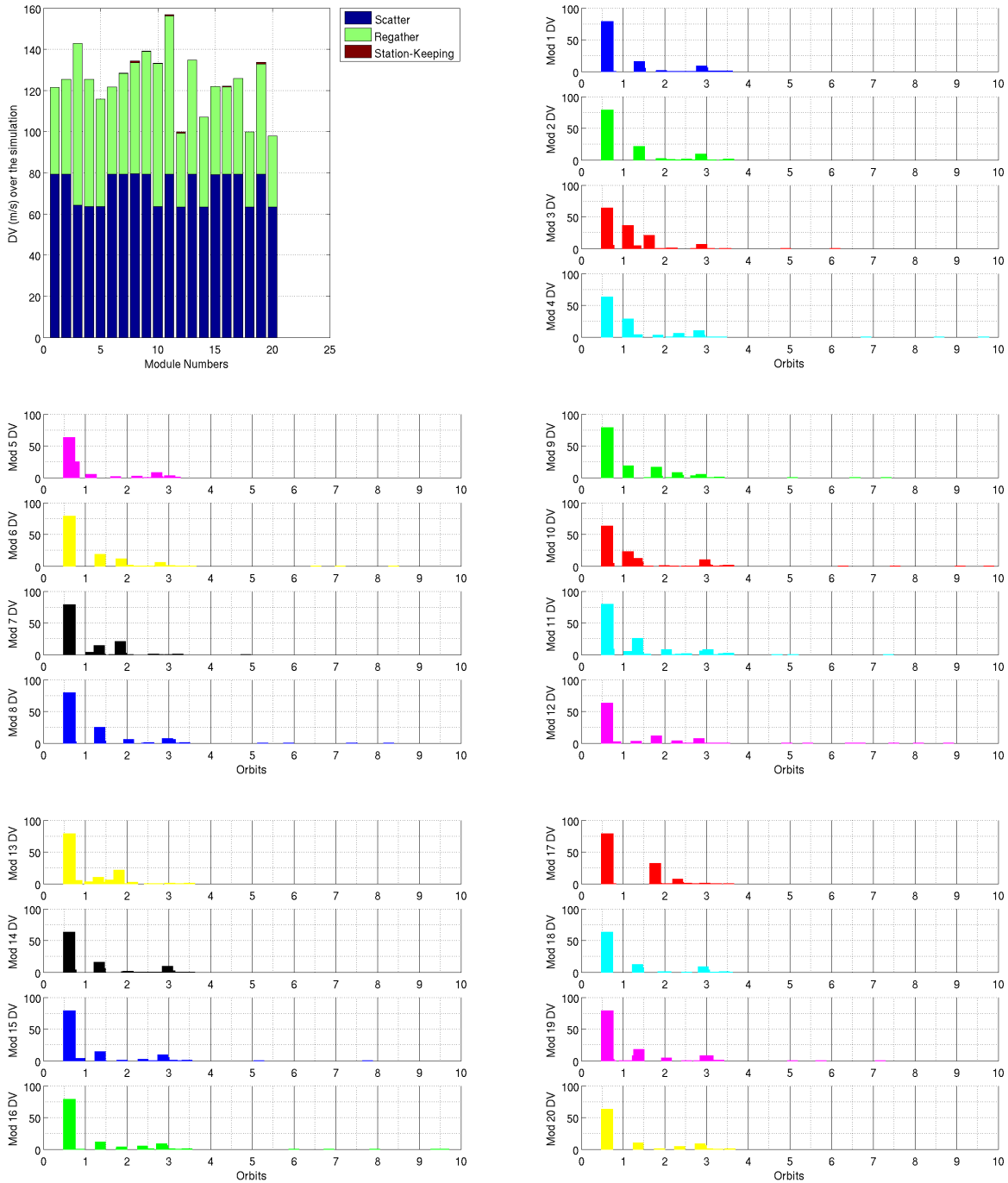


Figure 20: Twenty Module Cluster Scatter Trajectories

The module maneuver results are shown in Figure 21. The average per module  $\Delta V$  is 73.1 m/s for the initial scatter burn, 51.1 m/s for the post-scatter burns, and 0.2 m/s for station-keeping at the hold orbits. The average per module total  $\Delta V$  is 124.4 m/s. The total  $\Delta V$  results are higher than in the four and twelve module case due to the added IMD and KOZ constraints enforced across the cluster.



**Figure 21: Twenty Module Cluster Scatter Maneuvers**

The module trajectories are represented in terms of ROEs in Figure 22. The first subfigure depicts the module ROEs with respect to the initial cluster reference orbit, which is subsequently relocated 200 km downrange. The second subfigure depicts the relative trajectories in terms of the non-angular module ROEs with respect to the initial cluster leader (Module 1). The results are similar to the twelve-module case, but with broader distribution of initial scatter directions.

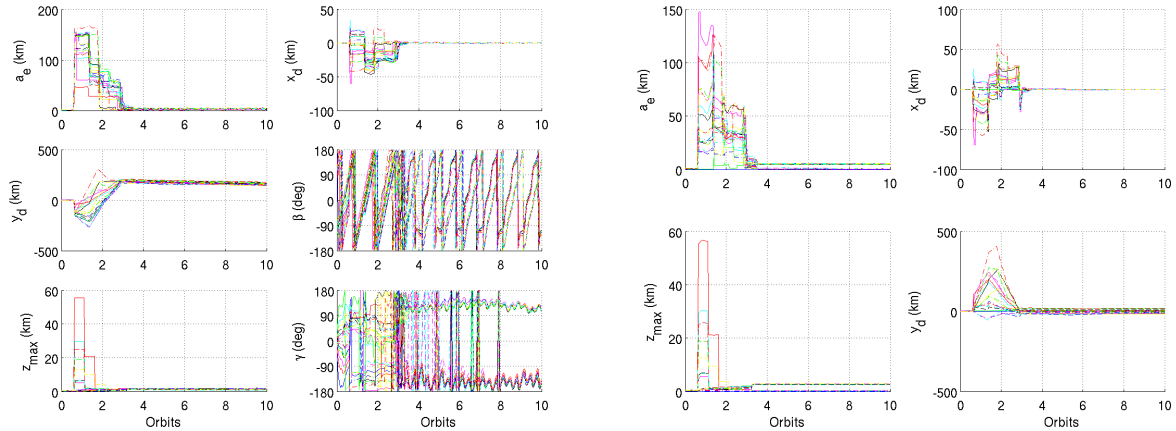


**Figure 22: Twenty Module Cluster Scatter ROEs with Respect to the Cluster Reference Orbit and the Leader Module**

The scatter performance results in terms of the IMDs and keep-out ranges are shown in Figure 23. The first subfigure shows the minimum IMD across the entire cluster, which stays above the configured threshold of 100 meters, as well as the maximum IMD. In general, the minimum IMD remains lower than the four and twelve module cases since there are more modules within the space of the cluster. The maximum IMD results are similar to the twelve module case.

The second subfigure shows the keep-out ranges at 5 minutes after the scatter command. In this case, there are 20 modules and 20 KOZs for a total of 400 keep-out range measurements. A few of the modules fall just below the 10 km keep-out range constraint as result of the time bias in executing scatter, which results in larger discrepancies between the presumed cluster configuration and the actual cluster configuration at the time of scatter. This is due to the increased complexity of computing maneuver plans for larger numbers of modules and a corresponding increase in the system sensitivity to targeting errors. The errors can be corrected by increasing the number of scatter pre-plans and pre-plan frequency during the computation of the pre-computed SMPs and thereby decreasing the time bias at the time of scatter execution.

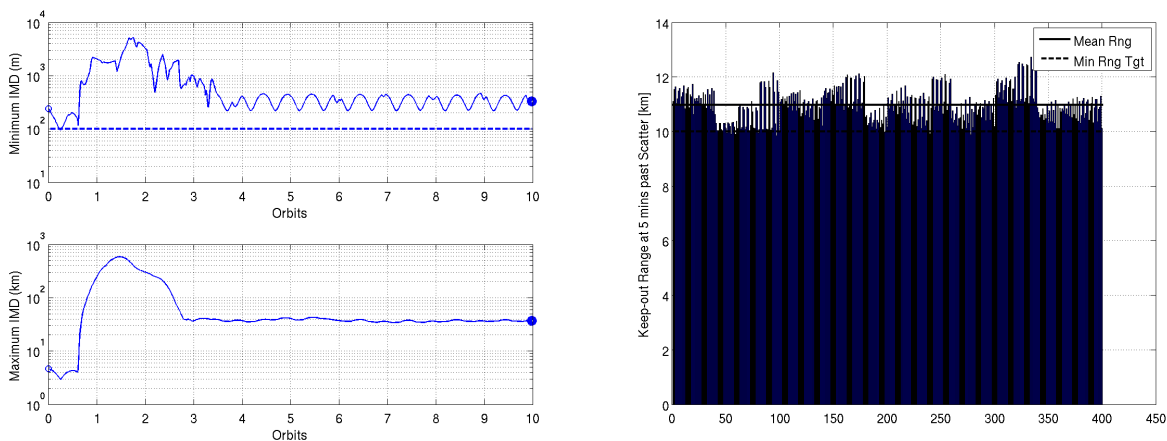


**Figure 23: Twenty Module Cluster Scatter Min and Max IMDs and Keep-Out Ranges**

### 3.2.3. Reduced Scatter Scenario

To demonstrate the scalability of CFA to varying scatter magnitudes, a reduced scatter scenario is presented. Such a reduced-scale scatter scenario has also been considered for application of an in-flight test of the scatter algorithms without the expense of high  $\Delta V$  use. The results for a four module scatter simulation are shown in Figures 24 - 27. The same configuration is used as in Section 3.1, but with a scaled down scatter using a 1 km keep-out constraint, 50 km down-range regather location, and reduced hold-orbits as configured in Eq. 11. This configuration of the hold-orbits effectively performs the scatter and regather phases in unison as discussed in Section 1.2.

$$\begin{aligned} a_e &= a_{e,target} \\ y_d &= y_{d,target} \\ z_{max} &= z_{max,target} \\ x_d &= x_{d,target} \\ \beta &= \beta_{target} \\ \gamma &= \gamma_{target} \end{aligned} \tag{11}$$

The initial scatter burn disperses the cluster beyond the 1 km keep-out constraint within 5 minutes and the transfer time is configured at 3 orbits. The hold orbits locations are 50 km down-range. The minimum IMD is maintained above 100 meters while a maximum IMD constraint is not enforced in this case. The simulation generates pre-planned SMPs at 5-minute intervals and the executed plan had a time bias of 140 seconds, which was corrected through a rotation of the  $\Delta V$  vectors as discussed in Section 2.3.

The module trajectories are shown in Figure 24 including a 3-dimensional viewpoint as well as in radial/in-track and radial/cross-track planes. Compared to the case in Section 3.1, the initial scatter trajectories are smaller in scale and more incorporated with the down-range post-scatter trajectories. The cluster does successfully arrive at the hold orbits/final configuration down-range from the initial cluster location.

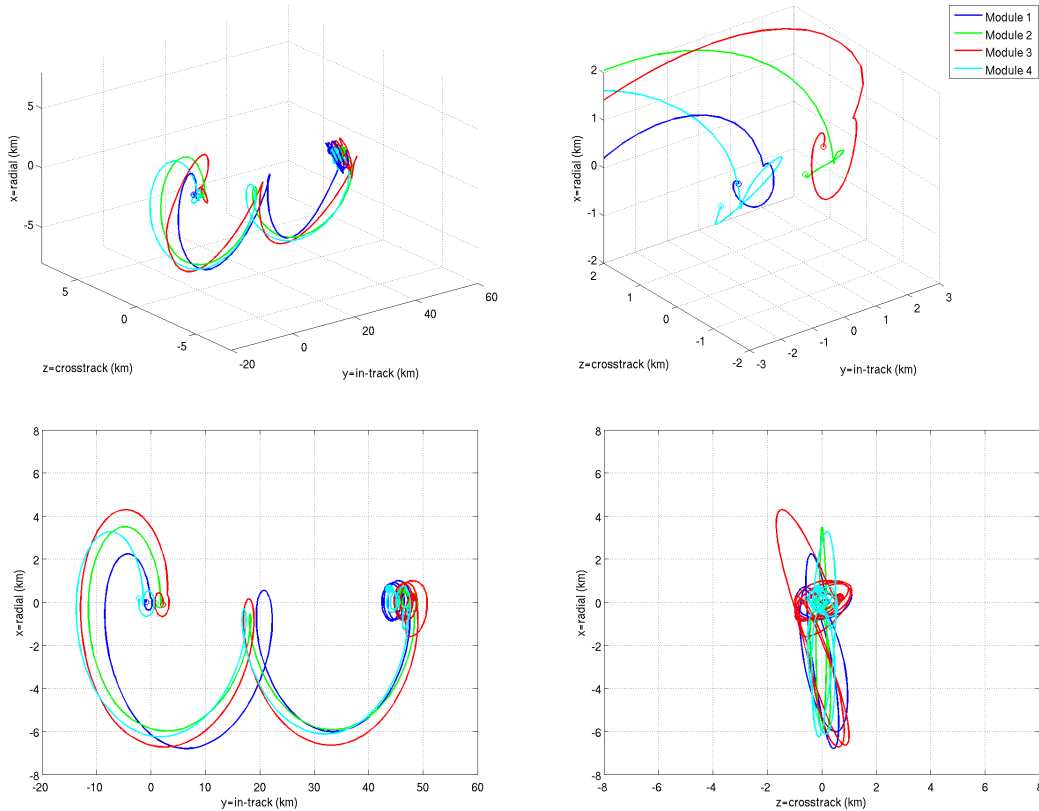


**Figure 24: Four Module Reduced Cluster Scatter Trajectories**

The module maneuver results are shown in Figure 25. As before, the magnitudes of the initial scatter burn and subsequent maneuvers vary depending on the module location within the cluster configuration and the trajectories followed to achieve the hold orbits. The scale of burn magnitudes is much reduced from the 10 km scatter case of Section 3.1. The average per module  $\Delta V$  is 4.9 m/s for the initial scatter burn, 5.2 m/s for the post-scatter burns, and 0.04 m/s for station-keeping at the hold orbits. The average per module total  $\Delta V$  is 10.14 m/s.

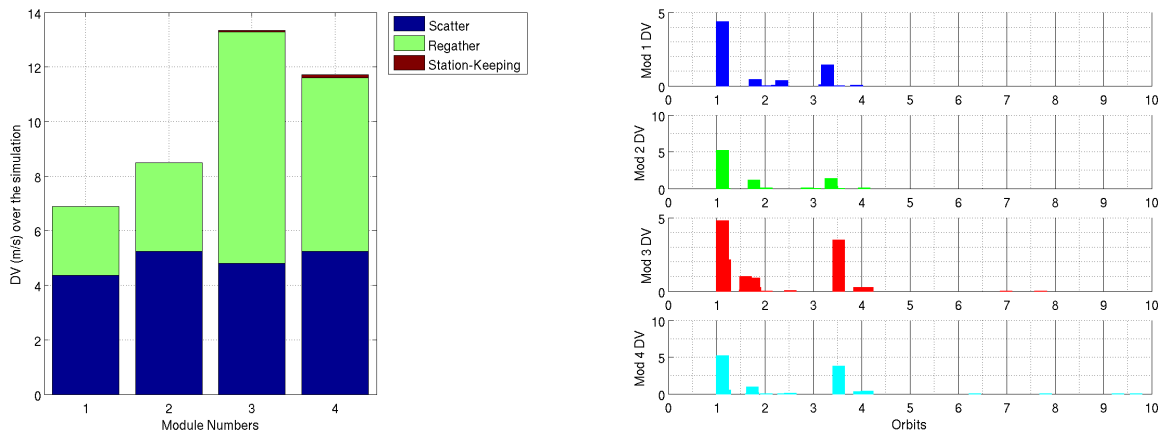


**Figure 25: Four Module Reduced Cluster Scatter Maneuvers**

The module trajectories are represented in terms of ROEs in Figure 26. The first subfigure depicts the module ROEs with respect to the initial cluster reference orbit, which is subsequently relocated 50 km downrange. The second subfigure depicts the relative trajectories in terms of the non-angular module ROEs with respect to the initial cluster leader (Module 1). The results are similar to the 10 km case in Figure 14, but at a smaller scale and regather location at 50 km down-range (expressed as  $y_d$  in terms of ROEs).

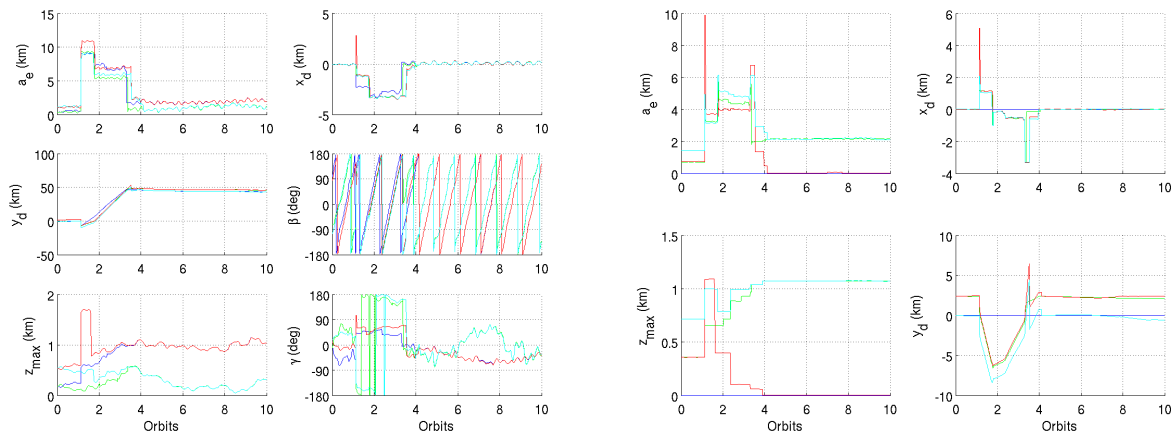


**Figure 26: Four Module Reduced Cluster Scatter ROEs with Respect to the Cluster Reference Orbit and the Leader Module**

The scatter performance results in terms of the IMDs and keep-out ranges are shown in Figure 27. All modules maintain safe separation while not drifting too far apart. Further, all modules successfully achieve the minimum 1 km range from each keep-out zone.

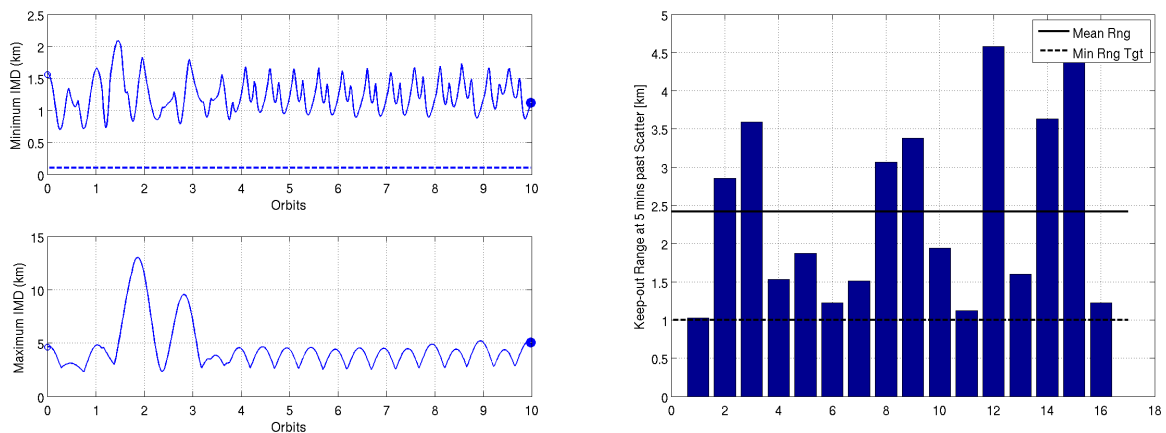


**Figure 27: Four Module Reduced Cluster Scatter Min and Max IMDs and Keep-Out Ranges**

#### 4. Conclusions

CFA was developed by Emergent Space Technologies to provide robust and scalable GN&C algorithms for cluster flight. In addition to potentially supporting nominal operations and station-

keeping, CFA integrates functionality that would scatter the cluster in response to a debris-like threat and regather it through a set of intermediary hold orbits. The CFA optimizes  $\Delta V$  consumption while maintaining mission and state constraints through a robust simulated annealing heuristic search algorithm and an underlying linear programming multi-burn solver. The maneuver planning software can account for initial, final, and interior state constraints while also minimizing the  $\Delta V$  consumption.

The performance of CFA in executing scatter and regather was demonstrated in simulation for varying numbers of modules and at two different magnitudes for the initial scatter distance constraint. The scatter results were presented in terms of the  $\Delta V$  requirements, module trajectories up to hold orbit arrival and the satisfaction of the scatter keep-out and passive safety IMD constraints. All the results showed reasonably good performance in achieving the scatter constraints with acceptable  $\Delta V$  and maintaining passive safety in terms of the minimum IMDs and communications range in terms of the maximum IMDs. Increasing the number of modules within the space of the cluster results in higher  $\Delta V$  and more dispersion among the module scatter trajectories. Increasing the number of modules also increases the sensitivity of the system to scatter execution errors, but nonetheless, the system response showed adequate scatter performance. Decreasing the magnitude of the scatter keep-out distance yields smaller burns with less total  $\Delta V$ . Such a reduced scale scatter serves as a viable method for verifying the on-orbit performance of the scatter algorithms before executing the full-scale scatter scenario.

Further analysis and system tuning is required to improve the overall scatter and regather performance in terms of targeting accuracy and  $\Delta V$ . Nonetheless, the system already demonstrates reasonably good performance and the potential ability to handle a wide-range of mission constraints, targets and scenarios. Further, the GN&C algorithms have been developed in such a manner as to promote their infusion into future cluster flight missions.

## **Acknowledgments**

The authors would like to thank Shaun Stewart and Eric Ferguson for their contributions toward the development of the CFA and in particular for their work on the CFA scatter and regather algorithms.

## **Distribution Statement “A” (Approved for Public Release, Distribution Unlimited)**

The views expressed are those of the authors and do not reflect the official policy or position of the Department of Defense or the U.S. Government.

## **5. References**

[1] Brown, O., Eremenko, P., and Bille, M., “Fractionated Space Architectures: Tracing the Path to Reality,” *Small Satellite Conference*, Logan, Utah, 2009.

[2] Hur-Diaz, S. and O’Connor, B., “Cluster Flight Application on System F6,” *Proceedings of the 24th International Symposium on Space Flight Dynamics*, Laurel, MD, May 2014.

- [3] United States Government, Defense Advanced Research Projects Agency, “System F6,” Oct 20, 2010 and amended, Solicitation Number: DARPA-BAA-11-01.
- [4] Brown, A., Ruschmann, M., Duffy, B., Ward, L., Hur-Diaz, S., Ferguson, E., and Stewart, S., “Simulated Annealing Maneuver Planner for Cluster Flight,” *Proceedings of the 24th International Symposium on Space Flight Dynamics*, Laurel, MD, May 2014.
- [5] Ruschmann, M., Duffy, B., de la Torre, R., and Hur-Diaz, S., “Efficient Station-Keeping Strategies for Cluster Flight,” *Proceedings of the 24th International Symposium on Space Flight Dynamics*, Laurel, MD, May 2014.
- [6] Gustafson, D. E. and Kriegsman, B. A., “A Guidance and Navigation System for Automatic Stationkeeping in Earth Orbit,” *Journal of Spacecraft and Rockets*, Vol. 10, No. 6, June 1973, pp. 369–376.
- [7] Lovell, T. A. and Tragesser, S. G., “Guidance for Relative Motion of Low Earth Orbit Spacecraft Based on Relative Orbit Elements,” *AIAA/AAS Astrodynamics Specialist Conference and Exhibit*, No. AIAA-2004-4988, American Institute of Aeronautics and Astronautics, Providence, RI, August 2004.
- [8] Lovell, T. A. and Tollefson, M. V., “Calculation of Impulsive Hovering Trajectories via Relative Orbit Elements,” *AIAA/AAS Astrodynamics Specialist Conference and Exhibit*, No. AAS 05-409, American Astronomical Society, San Diego, CA 92198, August 2005.
- [9] Gim, D.-W. and Alfriend, K. T., “State Transition Matrix of Relative Motion for the Perturbed Noncircular Reference Orbit,” *Journal of Guidance, Control and Dynamics*, Vol. 26, No. 6, 2003, pp. 956–971.
- [10] Gim, D.-W. and Alfriend, K. T., “Satellite Relative Motion using Differential Equinoctial Elements,” *Celestial Mechanics and Dynamical Astronomy*, Vol. 92, 2005, pp. 295–336.
- [11] Alfriend, K. T., Vadali, S. R., Gurfil, P., How, J. P., and Breger, L. S., *Spacecraft Formation Flying: Dynamics, Control and Navigation*, Elsevier, Kidlington, Oxford, UK, 1st ed., 2010.
- [12] Tillerson, M., Inalhan, G., and How, J. P., “Co-ordination and Control of Distributed Spacecraft Systems using Convex Optimization Techniques,” *International Journal of Robust and Nonlinear Control*, Vol. 12, 2002, pp. 207–242.
- [13] Dantzig, G. B., Orden, A., and Wolfe, P., “The Generalized Simplex Method for Minimizing a Linear Form Under Linear Inequality Restraints,” *Pacific Journal of Mathematics*, Vol. 5, No. 2, 1955, pp. 183–195.
- [14] Luenberger, D. and Ye, Y., *Linear and Nonlinear Programming*, Springer, 2nd ed., 1984.